HEALTH AND MEDICINE

Brain-targeted enzyme-loaded nanoparticles: A breach through the blood-brain barrier for enzyme replacement therapy in Krabbe disease

Ambra Del Grosso[1]*, Marianna Galliani[1,2]*, Lucia Angella[1], Melissa Santi[2], Ilaria Tonazzini[1], Gabriele Parlanti[1], Giovanni Signore[1,3†], Marco Cecchini[1†]

Lysosomal storage disorders (LSDs) result from an enzyme deficiency within lysosomes. The systemic administration of the missing enzyme, however, is not effective in the case of LSDs with central nervous system (CNS)-involvement. Here, an enzyme delivery system based on the encapsulation of cross-linked enzyme aggregates (CLEAs) into poly-(lactide-co-glycolide) (PLGA) nanoparticles (NPs) functionalized with brain targeting peptides (Ang2, g7 or Tf2) is demonstrated for Krabbe disease, a neurodegenerative LSD caused by galactosylceramidase (GALC) deficiency. We first synthesize and characterize Ang2-, g7- and Tf2-targeted GALC CLEA NPs. We study NP cell trafficking and capability to reinstate enzymatic activity in vitro. Then, we successfully test our formulations in the Twitcher mouse. We report enzymatic activity measurements in the nervous system and in accumulation districts upon intraperitoneal injections, demonstrating activity recovery in the brain up to the unaffected mice level. Together, these results open new therapeutic perspectives for all LSDs with major CNS-involvement.

INTRODUCTION

Lysosomal storage disorders (LSDs) are a large group of more than 70 clinically recognized metabolic disorders, which are individually rare but collectively common (1:5000 live births). They result for the most part from an enzyme deficiency within the lysosomes, which ultimately causes accumulation of undegraded substrates. This storage process leads to a broad spectrum of clinical manifestations depending on the specific substrate and site of accumulation. Most LSDs show widespread tissue and organ involvement, with brain, viscera, bone, and connective tissues usually affected. Brain disease is particularly prevalent, involving two-thirds of all LSDs (*1*).

Krabbe disease [KD or globoid cell leukodystrophy; Online Mendelian Inheritance in Man (OMIM) no. 245200] is a fatal pediatric neurodegenerative LSD caused by deficient activity of the enzyme galactosylceramidase (GALC; EC 3.2.1.46). GALC degrades galactosylceramide, a major component of myelin, and other terminal β-galactose–containing sphingolipids, including the cytotoxic D-galactosylsphingosine [psychosine (PSY)] (*2*). GALC loss of function causes increased PSY levels in neural tissues, leading to widespread degeneration of oligodendrocytes and Schwann cells and subsequent devastating demyelination. The disease is further characterized by central nervous system (CNS) infiltration of macrophages, which turn into multinucleated "globoid cells" (*3*).

In humans, KD is typically a neurodegenerative disease of early infancy (95% of known cases), but there are examples in which it has been diagnosed in older children and adults. The early infantile phenotype onset is typically within the first 6 months of life and leads to death by 2 years of age (*4*). No effective cure is currently available for KD. The only clinically applied method, which only delays symptom progression, is bone marrow transplantation (BMT). This treatment, however, is effective only if performed in the neonatal period, and the recruitment of an adult donor often takes too long for the treatment of a so rapidly progressive disorder. Yet, transplantation requires immunosuppressant therapies that may even worsen the conditions of the young patients (*5*).

Among other potential therapies, intracerebral gene therapy (GT) has recently yielded good results in experimental models such as mouse and dog (*6*, *7*). Nevertheless, both BMT and GT need time to engraft and create therapeutic effects, thus not allowing the effective prevention of early nervous system damage. For this reason, a therapy that could be promptly applied in the very first period after birth is required. To this end, systemic enzyme replacement therapy (ERT) would be the best option (*8*), but the presence of the blood-brain barrier (BBB) forbids the translocation of proteins like GALC (77 kDa) into the CNS. Only some low–molecular weight (<400–500 Da) and small lipophilic molecules are allowed to pass through the BBB (*9*).

In recent years, a lot of interest arose from the development of enzyme-loaded nanosystems, which may enhance the efficacy of ERT and minimize side effects using innovative and biocompatible nanomaterials. Enzyme encapsulation in biodegradable micelles, liposomes, and polymer- and lipid-based nanoparticles (NPs) can protect enzyme integrity and activity, eradicating some of the key limitations of ERT, including immunologic reactions and degradation (*8*). It can also enhance the pharmacological response by improving pharmacokinetics and pharmacodynamics and allowing for a controlled release of the payload (*10*). Moreover, the possibility of decorating the surface of the nanocarrier with targeting molecules (peptides, aptamers, and antibodies) promotes passage through biological barriers such as the BBB and blood-ocular barrier (*11*).

Among the investigated materials for NP synthesis, poly-(lactide-co-glycolide) (PLGA) has received special attention, being a biocompatible, nontoxic, and Food and Drug Administration–approved polymer for intravenous administration in humans (*12*). However, successful encapsulation of proteins and enzymes in PLGA NPs is still an open issue. We recently described (*13*) a new encapsulation strategy that allows loading enzymes with excellent efficiency and activity retention.

[1]NEST, Istituto Nanoscienze-CNR and Scuola Normale Superiore, Piazza San Silvestro 12, 56127 Pisa, Italy. [2]Center for Nanotechnology Innovation@NEST, Piazza San Silvestro 12, 56127 Pisa, Italy. [3]Fondazione Pisana per la Scienza ONLUS, 56017 Pisa, Italy.
*These authors contributed equally to this work.
†Corresponding author. Email: marco.cecchini@nano.cnr.it (M.C.); g.signore@fpscience.it (G.S.)

In particular, we reported a synthesis method for a new enzyme delivery platform based on cross-linked enzyme aggregates (CLEAs) encapsulation into PLGA NPs. We demonstrated that this system allows encapsulation of different enzymes (PPT1, GALC, and glucosidase) with excellent activity retention. Delivery efficiency and enzyme activity recovery were validated in vitro using neuronal ceroid-lipofuscinosis type 1 (NCL1) primary fibroblasts.

In the present work, we focused on GALC for testing in vivo enzyme delivery into the brain. To this end, we synthesized and fully characterized three new formulations of GALC CLEA–loaded PLGA NPs. These NPs were functionalized with targeting peptides [Angiopep-2 (Ang2) (*14*), g7 (*15*), or transferrin binding (Tf2) peptides (*16*)], aimed to allow NPs to pass the BBB. At first, we studied NP cell uptake and trafficking and their capability to reinstate enzymatic activity in murine model cells and in fibroblasts from patients with KD. Then, we tested our nanosystem in vivo in the Twitcher (TWI) mouse, the spontaneous mouse model of the KD (*17*). We evaluated enzymatic activity recovery 4 hours after NP intraperitoneal injection in different organs of the CNS and peripheral nervous system (PNS), as well as in typical accumulation districts. Moreover, we assessed the presence of targeted NPs in extracted brains and livers by means of confocal fluorescence microscopy.

RESULTS

Synthesis and characterization of targeted GALC CLEA NPs

For these experiments, three targeted versions of GALC CLEA–loaded NPs were synthesized, each decorated with a different peptide for CNS targeting (Fig. 1A). GALC CLEA NPs were produced with a two-step protocol previously developed by our group and functionalized with the targeting peptides Ang2, g7, or Tf2 with a preformulation approach including a peptide-modified PLGA in the formulation. First, Ang2, g7, and Tf2 peptides were synthesized by solid phase synthesis. Then,

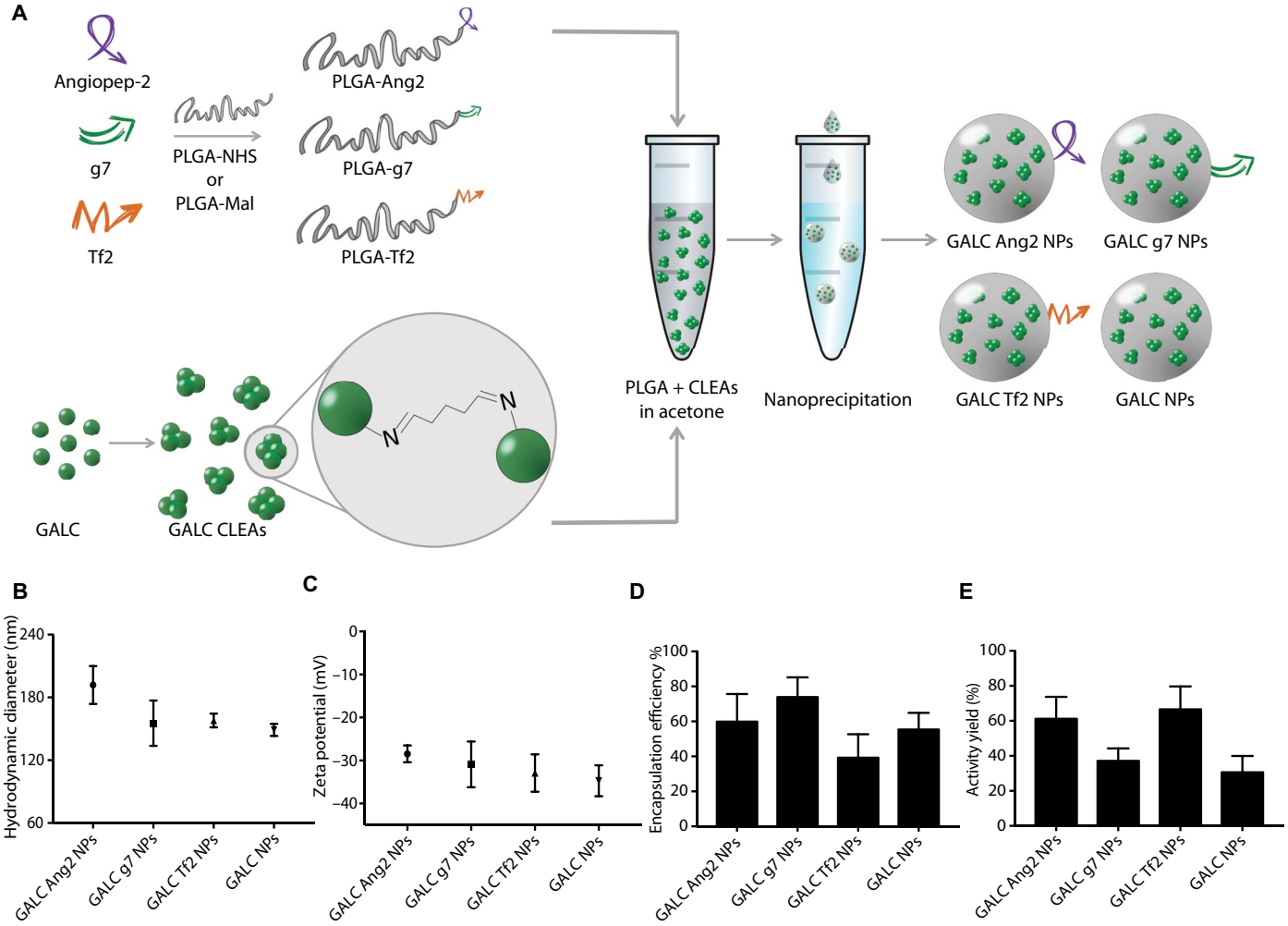

Fig. 1. Targeted GALC CLEA NP synthesis and characterization. (**A**) Graphical summary of the experiment. Peptide-modified PLGA was produced by covalent linking of each peptide to a previously activated form of PLGA. GALC CLEAs were obtained by precipitation of GALC in acetone in the presence of glutaraldehyde, resulting in Schiff base formation between enzyme molecules. Last, targeted GALC CLEA NPs were obtained by nanoprecipitation. (**B**) Hydrodynamic Diameter of GALC CLEA NPs. Error bars represent the SEM of four independently synthesized NP batches. (**C**) Zeta potential of GALC CLEA NPs. Error bars represent the SEM of four independently synthesized NP batches. (**D**) Encapsulation efficiency of GALC CLEA NPs. Encapsulation efficiency is expressed as percentage of encapsulated GALC with respect to the amount of enzyme used in each synthesis. Error bars represent the SEM of four independently synthesized NP batches. (**E**) Activity yield of GALC CLEA NPs. Activity yield is expressed as percentage of specific activity (nanomole substrate hydrolyzed in 1 hour by 1 μg of enzyme) with respect to the free unaltered enzyme. Error bars represent the SEM of four independently synthesized NP batches.

each peptide was covalently attached to PLGA, exploiting the terminal carboxylic acid on the polymer (*18*). Precisely, cysteine-terminated Ang2 and Tf2 were linked to maleimide-activated PLGA, whereas amine-terminated g7 was attached to *N*-hydroxysuccinimide (NHS)–activated PLGA. Next, GALC CLEAs were first produced by precipitation of the enzyme in acetone in the presence of glutaraldehyde, resulting in Schiff base formation and subsequent cross-linking of the precipitated enzyme. Then, GALC CLEAs were encapsulated into targeted PLGA NPs by nanoprecipitation. To this end, GALC CLEAs, PLGA, and peptide-modified PLGA were mixed in acetone and added dropwise to an aqueous solution of sodium cholate. In this process, PLGA spontaneously precipitated as acetone diffused into water, encapsulating CLEAs into NPs that could be collected by centrifugation. Control nontargeted GALC CLEA–loaded NPs were produced by encapsulation of CLEAs in nonmodified PLGA NPs.

The main features of GALC CLEA NPs are reported in Fig. 1 (B to E). All the produced NPs showed a hydrodynamic diameter below 200 nm with small differences among the NP types, with GALC Ang2 NPs and nontargeted NPs displaying the largest (191 ± 18 nm) and the smallest (149 ± 6 nm) diameters, respectively. On the contrary, the surface zeta potential was rather uniform among all NP types (around −30 mV). GALC CLEAs were successfully encapsulated by all the NP formulations, with encapsulation efficiencies ranging from 40 to 75%. The NP formulation showing the best encapsulation efficiency was GALC g7 NPs, whereas GALC Tf2 NPs led to the greatest enzyme loss during synthesis. The activity yield also varied among the batches, with GALC Ang2 and GALC Tf2 NPs being the formulations with highest GALC activity preservation.

Intracellular delivery of targeted NPs

Before testing the efficacy of GALC CLEA NP–mediated ERT, we explored their cellular uptake and intracellular trafficking in primary fibroblasts extracted from TWI and wild-type (WT) mice by means of confocal microscopy and colocalization analysis. In particular, we investigated whether GALC CLEA NPs could be endocytosed by cells and reach the right intracellular target of GALC, which is the lysosome (*19*, *20*). To this end, we produced a dual fluorescently labeled version of each NP formulation used in this study (Ang2-, g7-, or Tf2-targeted NPs and nontargeted NPs) by encapsulating ATTO 488–labeled GALC CLEAs into ATTO 633–tagged PLGA NPs. We then incubated either TWI or WT fibroblasts with NPs for 4 hours. Cells were subsequently washed and incubated in fresh medium; after 24 hours, cells were fixed and stained for lysosomes and nuclei. Four-color confocal fluorescence microscopy was lastly carried out to assess the intracellular localization of both NPs and GALC independently (Fig. 2A). A first visual image analysis showed that both GALC and NPs extensively colocalized in lysosomes of both TWI (Fig. 2B) and WT (fig. S1) fibroblasts. Moreover, the enzyme was found in lysosomes independently from the presence and the identity of the targeting ligand in TWI and WT cells as well. These qualitative results were confirmed by a quantitative colocalization analysis that we performed by calculating the Manders' coefficient for GALC/lysosomes and NP/lysosomes. As shown in Fig. 2C, this coefficient was around 0.8 both for GALC/lysosomes and PLGA/lysosomes overlap, proving that the enzyme and NPs are highly colocalized with the lysosomes. Overall, these data demonstrate that GALC CLEA NPs are effectively endocytosed by GALC-deficient cells into lysosomes, the desired cell compartment allowing for optimal GALC action.

NP-mediated enzymatic activity recovery in vitro

After the demonstration of the capability of GALC CLEA NPs to reach cell lysosomes, we tested whether they could restore GALC enzymatic activity in deficient cells in vitro. To pursue this aim, we used murine TWI and WT cells and fibroblasts from patients with KD and healthy donors (HDs) (see Material and Methods for details on cell culture and treatments).

First, we performed a dose-response enzymatic recovery experiment in GALC-deficient (TWI) murine cells to find a useful dose range to approximately reach the GALC enzymatic activity of healthy cells. WT cells were used as healthy control. Specifically, we treated TWI cells with increasing doses of targeted or nontargeted GALC CLEA NPs, which corresponded to the following doses of enzyme: 0.75, 1.5, 3.0, and 6.0 U. Intracellular GALC activity was tested 4 hours after treatments. Control TWI cells were also treated with equivalent doses of free recombinant murine GALC (rm-GALC). See Fig. 3A for an overview of the experimental plan.

The first important observation was that the administration of enzyme-loaded NPs led to substantial GALC activity (>25% with respect to WT cells) within TWI cells regardless the tested formulation/dose. More specifically, the enzymatic activity increased with the dose in all cases (Fig. 3B). Focusing on targeted formulations, the trend was quite similar for Ang2 and g7 NPs. In both cases, only the 0.75-U dose returned a GALC intracellular activity significantly different from that of WT (taken as 100%) cells. With the dose of 1.5 U of NPs, instead, GALC activity was approximately 50% of the WT conditions, and by administrating 3 U, the activity reached that of WT cells. At the maximal dose (6 U), the WT activity was even exceeded. Tf2 NPs behaved similarly to Ang2 and g7 NPs at the lowest and the highest doses, whereas intermediate doses yielded similar recovery to the lowest dose. Expectedly, nontargeted NPs were internalized with efficiency comparable to targeted NPs being significantly different from the WT conditions for the two lowest doses. The third dose recovered the WT activity, and the last one overexceeded it. Cells treated with free GALC showed increased activity upon treatment, but this effect was less pronounced than in the case of NPs. NPs not loaded with GALC CLEAs (empty NPs in Fig. 3C) did not yield any detectable enzymatic activity. The basal GALC activity of TWI fibroblasts (TWI-UT in Fig. 3C) was approximately indistinguishable from the background level of the experimental setting, as already reported (*21*).

Given that the 3-U dose of NPs demonstrated the ability to successfully recover the WT activity in most of the formulations without overexceeding the WT level, it was selected for the subsequent time-response experiments. In this case, both murine and human cells were treated with targeted and nontargeted NPs or with free rm-GALC. After 4 hours, cells were washed and added with fresh medium. GALC enzymatic activity was then assayed 24 or 96 hours after treatments (see the experimental plan in Fig. 4A).

Murine cells treated with targeted or nontargeted NPs successfully maintained approximately the WT enzymatic activity for 24 and 96 hours, except for nontargeted NPs at the time point of 96 hours. Moreover, activity promoted by g7- and Tf2-targeted NPs significantly went beyond the WT levels. The rm-GALC–treated cells, instead, reached the WT activity only after 96 hours and only in this case we measured a significant difference between 24 and 96 hours within the same treatment.

The same experiments were carried out with KD patient fibroblasts having the common 30-kb deletion in the GALC gene (30kbΔ in Fig. 4D). Cells treated with targeted or nontargeted NPs showed similar

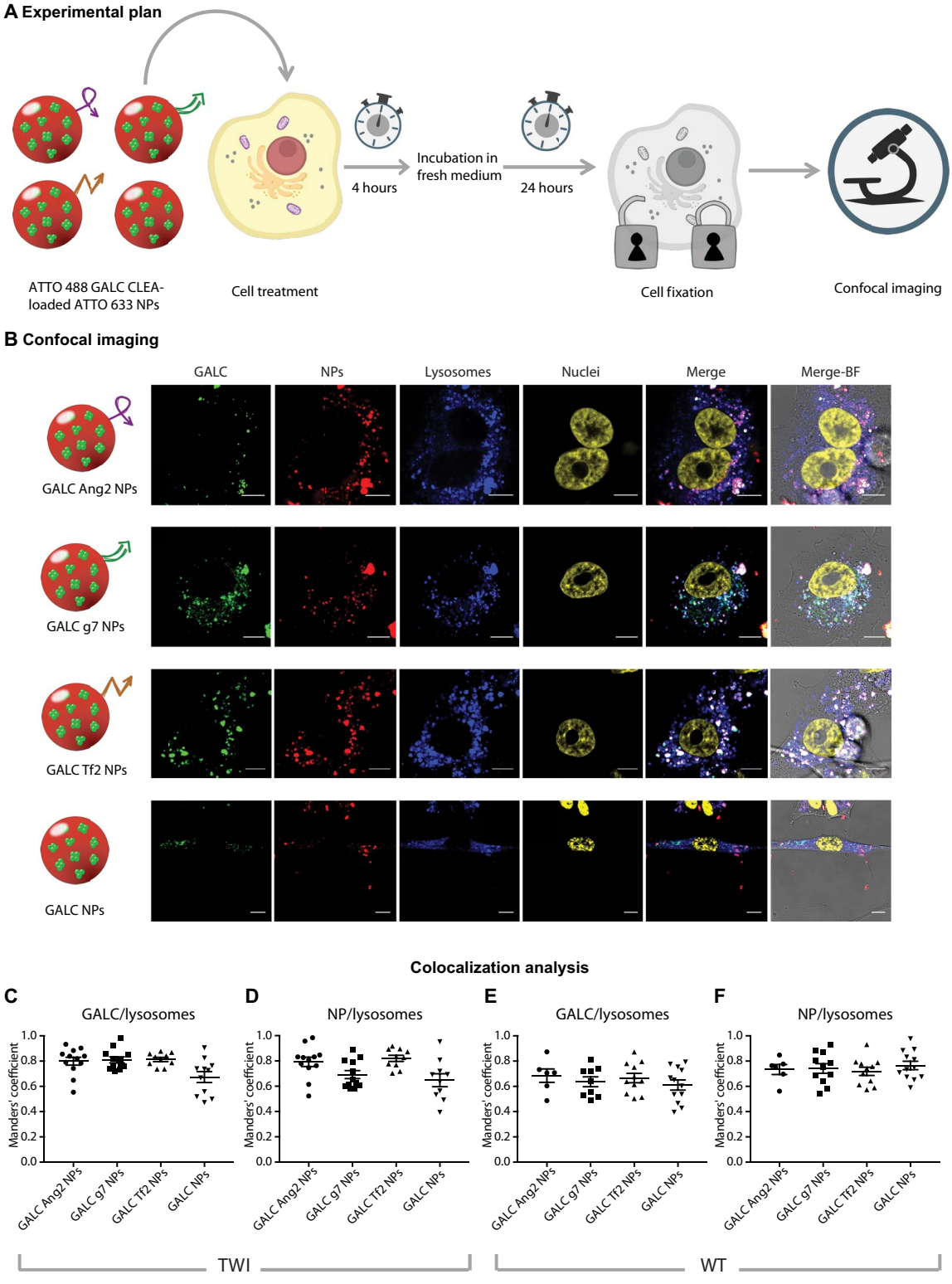

Fig. 2. Intracellular localization of targeted GALC CLEA NPs. (**A**) Graphical summary of the experiment. TWI or WT primary fibroblasts were incubated with fluorescently labeled ATTO 488 GALC CLEA-loaded ATTO 633 NPs for 4 hours and then washed and added with fresh medium. After 24 hours, cell lysosomes were stained, and cells were fixed and imaged with a confocal microscope. (**B**) Confocal imaging. Representative confocal images of TWI fibroblasts treated with fluorescently labeled GALC Ang2 NPs, GALC g7 NPs, GALC Tf2 NPs, or GALC NPs. From the left to the right column: GALC (green, stained with ATTO 488), NPs (red, stained with ATTO 633), lysosomes (blue, stained with LysoTracker Red DND-99), nuclei (yellow, stained with DAPI), superimposition of GALC, NPs, lysosomes, and nuclei fluorescence and superimposition of all channels with bright-field (BF) images. Scale bars, 10 μm. (**C** and **D**) Colocalization analysis. Manders' coefficient of GALC/lysosomes and NPs/lysosomes overlap in TWI cells treated with GALC CLEA NPs. (**E** and **F**) Manders' coefficient of GALC/lysosomes and NPs/lysosomes overlap in WT cells treated with GALC CLEA NPs.

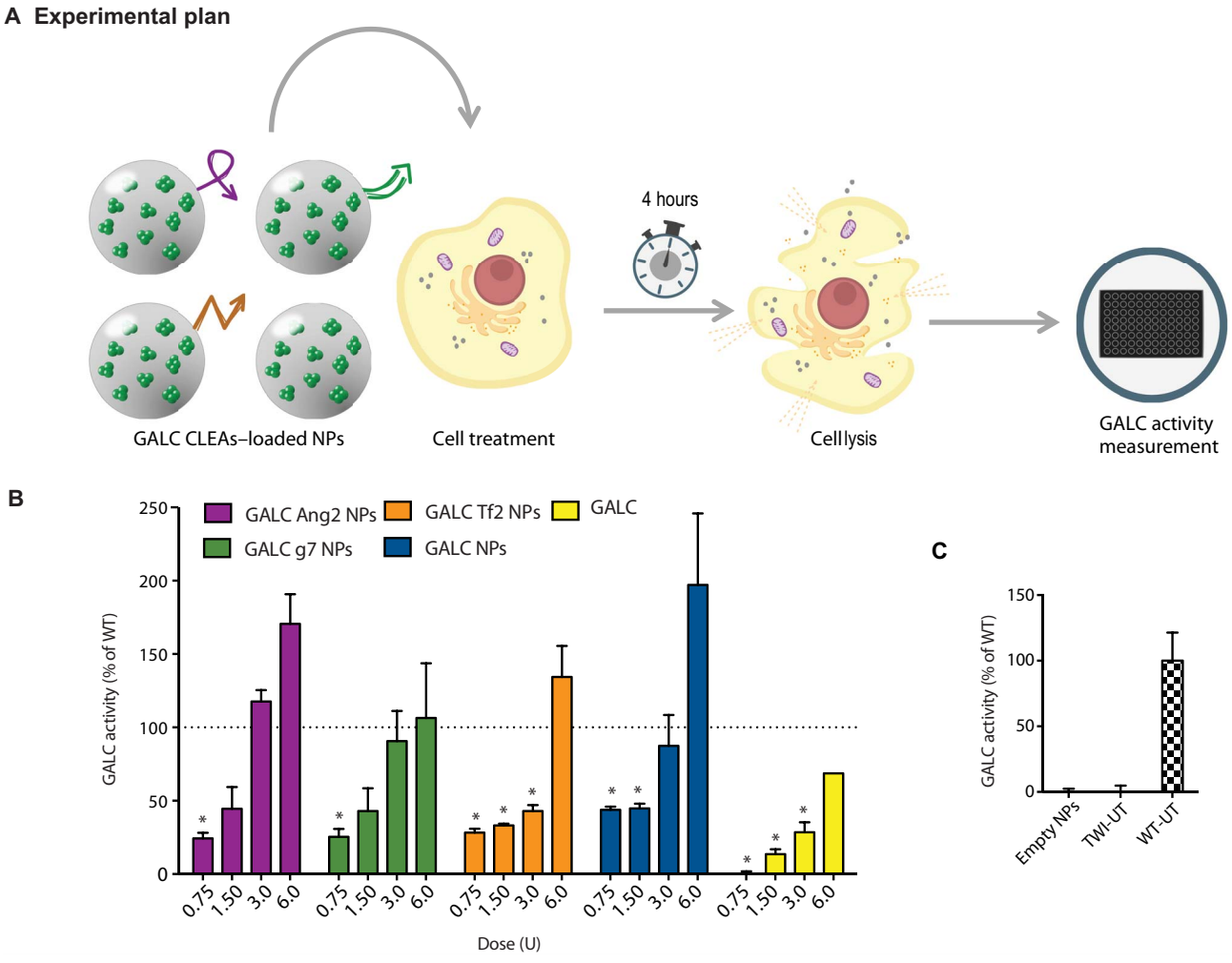

Fig. 3. In vitro ERT: Dose-response experiment. (**A**) Graphical summary of the experiment. GALC-deficient primary fibroblasts (derived from TWI mice) were treated with GALC CLEA NPs. After 4 hours, GALC activity was measured on cellular lysates by 6-hexadecanoylamino-4-methylumbelliferyl-β-D-galactopyranoside (HMU-βGal) assay. (**B**) Dose-response experiment results. Cells were treated with targeted GALC CLEA NPs (GALC Ang2 NPs, GALC g7 NPs, or GALC Tf2 NPs), with nontargeted NPs (GALC CLEA NPs), or with the free rm-GALC (GALC). For every treatment, four doses were tested: 0.75, 1.50, 3.0, and 6.0 U [unit (U) = amount of enzyme that catalyzes 1 nmol of substrate per hour]. Results are expressed in unit per microgram and reported in percentage of the activity of the WT cells [(U/μg) = unit of enzyme per microgram of cell lysate]. *$P < 0.05$ specific treatment versus WT, one-way analysis of variance (ANOVA) (Dunnett's multiple-comparisons test), means ± SEM ($n = 3$). (**C**) Controls. For control, NPs nonloaded with GALC CLEAs (empty NPs) were also administered to the cells. WT- and TWI-untreated cells activity is also showed. Means ± SEM ($n = 3$).

activity to that of cells from HDs, except for those treated with g7- and Tf2-targeted NPs after both 24 and 96 hours, whose activities were significantly higher than the HD level. In the case of Tf2-targeted and nontargeted NPs, the activity resulted significantly higher after 96 hours compared to the 24-hour time point. Free rm-GALC–treated cells reached HD levels after 24 hours, but activity decreased with time, resulting in an opposite trend with respect to what was reported for the murine cells. The GALC activity of TWI and 30kbΔ cells was not discernable from the background at both time points. (Fig. 4, C and E). Together, these data demonstrate that GALC CLEA NPs maintain enzymatic activity upon cellular uptake and that they can completely reinstate GALC activity in TWI and KD patient cells as well.

NP-mediated enzymatic activity recovery in vivo

The next step was to test GALC CLEA NPs as therapeutic agents for enzymatic activity recovery in the brain of the TWI mouse. Before these experiments, the stability of the encapsulated enzyme in the presence of serum proteins was evaluated. To this end, to mimic a biological fluid, we incubated all kinds of NPs used in the study in a medium containing 50% fetal bovine serum and studied the kinetics of drug release. At specific time points, we measured the GALC activity both in the medium (due to the released enzyme) and within the NP (due to the enzyme not released yet). The release kinetics of GALC CLEAs was only slightly affected by the presence of serum proteins. Specifically, in the presence of proteins, around 50% of the payload were released within the first 24 hours (fig. S3A), whereas in serum-free medium, NPs could retain 60% of the enzyme in the same time window (fig. S3B). One should also note that the incubation of free nonencapsulated GALC in the presence of serum proteins led to a marked loss of activity already after few hours. This confirms that although the protein corona had an influence on the release kinetics of the payload, as expected (*22*), the encapsulation into NPs is a fundamental requirement not only to allow the right targeting but also to consent the enzyme to reach the desired target in its active form. Then, to lastly demonstrate the delivery

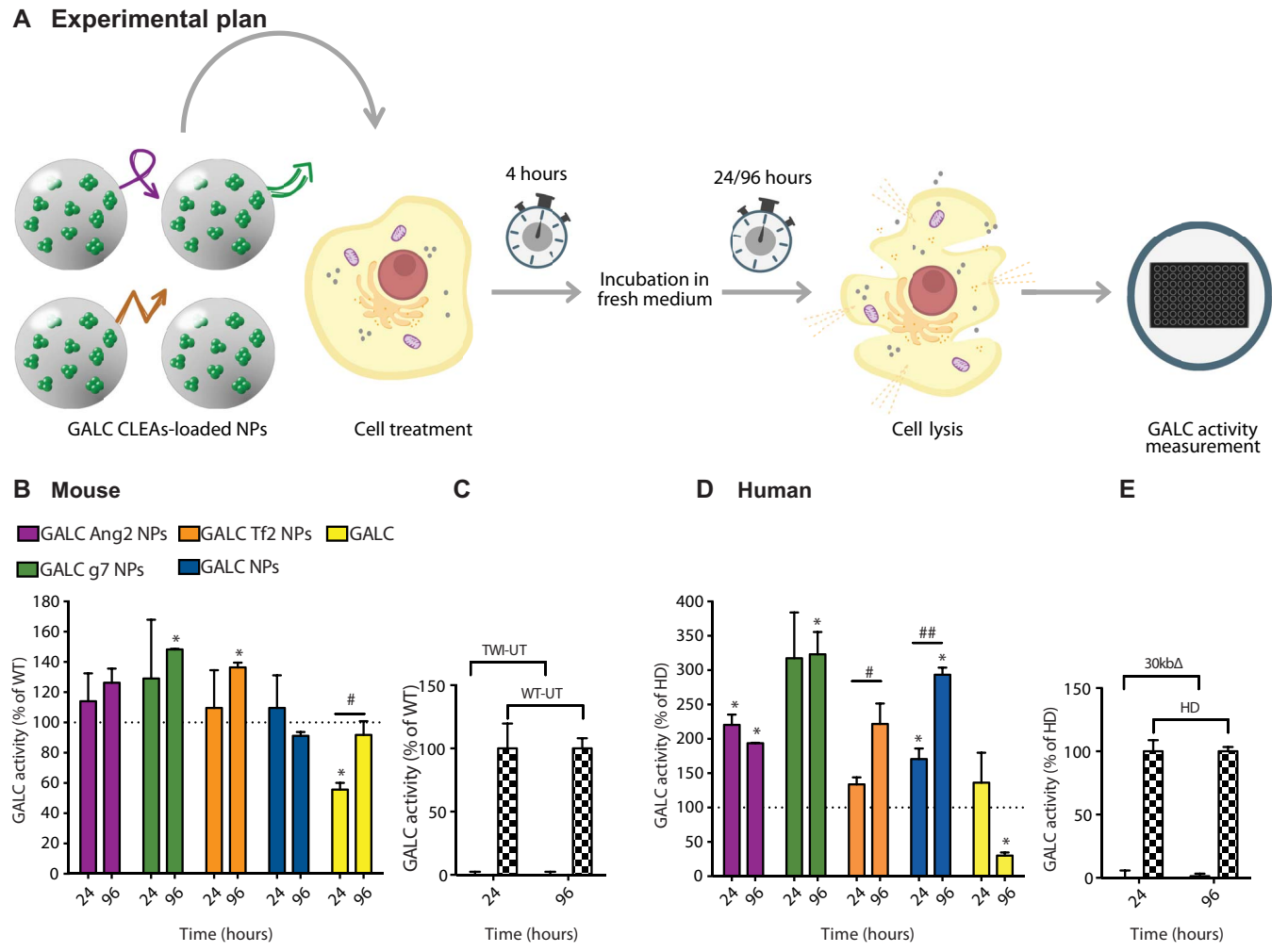

Fig. 4. In vitro: ERT time-response experiment. (**A**) Graphical summary of the experiment. GALC-deficient primary murine (from TWI mice) and human (from patients with KD with GALC 30kbΔ) fibroblasts were treated with a single dose [3.0 U; unit (U) = amount of enzyme that catalyzes 1 nmol of substrate/hour] of targeted GALC CLEA NPs (GALC Ang2 NPs, GALC g7 NPs, or GALC Tf2 NPs), nontargeted NPs (GALC CLEA NPs), or with the free rm-GALC (GALC). Four hours later, cells were incubated with fresh medium. GALC activity was measured in the cell lysates 24 or 96 hours later by HMU-βGal assay. (**B**) NPs mediated ERT in GALC deficient mouse cells. Results are expressed in unit per microgram and reported as percentage of the activity of the WT cells (U/μg = unit of enzyme per microgram of cell lysate). *P < 0.05 specific treatment versus WT, one-way ANOVA (Dunnett's multiple comparisons test). #P < 0.05 GALC 96 hours versus GALC 24 hours, Student's t test, means ± SEM (n = 3). (**C**) Controls. WT and TWI untreated cells activity at 24 and 96 hours. Means ± SEM (n = 3). (**D**) NPs mediated ERT in GALC deficient human cells. Results are expressed in unit per microgram and reported in percentage of the activity of the healthy (HD, human donor) cells (U/μg = unit of enzyme per microgram of cell lysate). *P < 0.05 specific treatment versus WT, one-way ANOVA (Dunnett's multiple comparisons test). #P < 0.05 GALC Tf2 NPs 96 hours versus GALC Tf2 NPs 24 hours and ##P < 0.01 GALC NPs 96 hours versus GALC NPs 24 hours, Student's t test, means ± SEM (n = 3). (**E**) Controls. HD and 30kbΔ untreated cells activity at 24 and 96 hours. Means ± SEM (n = 3).

of active enzyme to the brain in vivo, the mice were systematically administered with the NPs, and the presence of active GALC in key CNS and PNS organs was evaluated by means of enzymatic activity measurement and confocal fluorescence microscopy. This experiment was carried out in young mice (P19 to P21) before symptom onset (*17*).

Thus, we first synthesized targeted and nontargeted GALC CLEA NPs labeled with the fluorophore ATTO 633 to allow visualization of NPs in extracted tissues (see the experimental plan in Fig. 5A and Materials and Methods for further details). Then, TWI mice were treated with NPs or with free rm-GALC via a single intraperitoneal injection. After 4 hours, mice were euthanized by transcardial phosphate-buffered saline (PBS) perfusion to thoroughly wash blood vessels, and organs were extracted for characterization. In particular, we investigated GALC activity in representative organs of the CNS and PNS (brain and spinal cord and sciatic nerves, respectively) and in typical accumulation organs (liver and kidneys). GALC activity was assayed and compared with the activity of the same organs extracted from control mice [nontreated WT mice (WT-UT), nontreated TWI mice (TWI-UT), and nontreated heterozygous (HET) mice (HET-UT) mice; see the legend in Fig. 5B]. The presence of NPs was then investigated by fluorescence confocal imaging in paraformaldehyde (PFA)–fixed tissues. Mice were divided in five experimental groups (see again legend in Fig. 5B): WT-UT, HET-UT, TWI-UT, TWI treated with targeted NPs (TWI Targ-NPs), and TWI treated with nontargeted NPs or with rm-GALC (TWI Controls). To further assess the reproducibility of results, we tested two independently synthesized NP batches for each NP type (lot a and lot b; Fig. 5B).

As reported in Fig. 5C, GALC activity raised up to the 42 ± 4% of the activity measured for WT-UT in the brains of TWI mice treated with

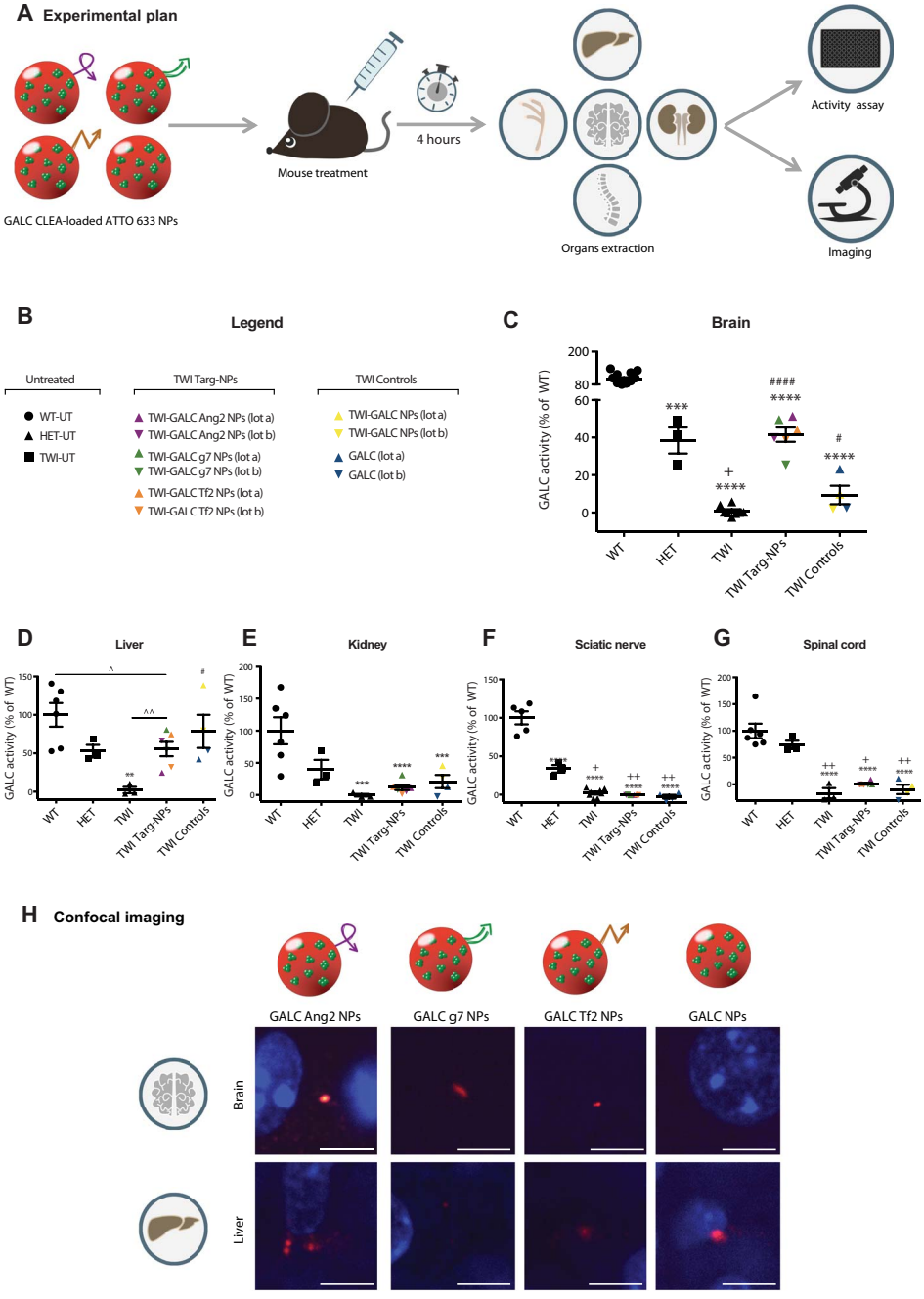

Fig. 5. In vivo NP mediated ERT in the TWI mice. (**A**) Graphical summary of the experiment. TWI mice were treated with targeted GALC CLEA ATTO 633 NPs (GALC Ang2 NPs, GALC g7 NPs, or GALC Tf2 NPs), nontargeted GALC CLEA ATTO 633 NPs (GALC CLEA NPs), or with the free rm-GALC (GALC). Four hours later mice were euthanized, and GALC activity was assayed in extracted brain, sciatic nerves, spinal cord, kidneys, and liver by HMU-βGal assay. (**B**) Legend. Untreated: WT (WT-UT), heterozygous (HET-UT), and TWI (TWI-UT). Targeted GALC CLEA ATTO 633 NPs (TWI Targ-NPs): TWI-GALC Ang2 NPs (lot a and lot b), TWI-GALC g7 NPs (lot a and lot b), and TWI-GALC Tf2 NPs (lot a and lot b). Control treatments (TWI Controls): GALC CLEA ATTO 633 NPs (TWI-GALC NPs lot a and lot b) and free rm-GALC (GALC-lot a and lot b). (**C**) Brain GALC activity. ***$P < 0.001$ HET versus WT; ****$P < 0.0001$ TWI, TWI Targ-NPs, and TWI Controls versus WT; +$P < 0.05$ TWI versus HET; #$P < 0.05$ TWI Controls versus TWI; ####$P < 0.0001$ TWI Targ-NPs versus TWI one-way ANOVA (Tukey's test). Means ± SEM ($n = 3$ to 12 per group). (**D**) Liver GALC activity. **$P < 0.01$ TWI versus WT and #$P < 0.05$ TWI Controls versus TWI, one-way ANOVA (Tukey's test). ^$P < 0.05$ TWI Targ-NPs versus WT and ^^$P < 0.01$ TWI Targ-NPs versus TWI, Student's *t* test. Means ± SEM ($n = 3$ to 6 per group). (**E**) Kidney GALC activity. ***$P < 0.001$ TWI and TWI Controls versus WT and ****$P < 0.0001$ TWI Targ-NPs versus WT, one-way ANOVA (Tukey's test). Means ± SEM ($n = 3$ to 6 per group). (**F**) Sciatic nerve GALC activity. Results are expressed in unit per microgram and reported as percentage of the WT activity (U/μg = unit of enzyme per microgram of cell lysate). ****$P < 0.0001$ all groups versus WT, +$P < 0.05$ TWI versus HET, ++$P < 0.01$ WT, TWI Targ-NPs and TWI Controls versus HET, one-way ANOVA (Tukey's test). Means ± SEM ($n = 3$ to 8 per group). (**G**) Spinal cord GALC activity. ****$P < 0.0001$ HET, TWI Targ-NPs and TWI Controls versus WT, +$P < 0.05$ TWI Targ-NPs versus HET, and ++$P < 0.01$ TWI and TWI Controls versus HET, one-way ANOVA (Tukey's test). Means ± SEM ($n = 3$ to 7 per group). (C to G) Results are expressed in unit per microgram and reported in percentage of the WT activity (U/μg = unit of enzyme per microgram of cell lysate). (**H**) Confocal imaging. Representative confocal images of brains and livers of the treated TWI mice. NPs are shown in red in the brains of the mice administered with the functionalized targeted GALC CLEA ATTO 633 NPs (GALC Ang2 NPs, GALC g7 NPs, or GALC Tf2 NPs), while they are not present in the brain of the mice treated with the nontargeted GALC CLEA ATTO 633 NPs (GALC CLEA NPs). All livers present NPs. Scale bars, 5 μm.

targeted NPs. This value was significantly higher with respect to the approximately undetectable activity of the TWI-UT and reached the value of the HET-UT (45 ± 8%), which represents a condition for which the disease does not manifest. TWI Controls instead reported a lower median value not significantly different from the TWI-UT, indicating that GALC could not be transported into the brain.

We detected a significantly higher activity in the liver in both TWI Targ-NPs and TWI Control mice (Fig. 5D) with respect to the TWI-UT. This activity had likewise a higher median value for TWI Controls with respect to TWI Targ-NPs, indicating greater liver accumulation in the case of nontargeted NPs and of rm-GALC.

Kidneys showed a similar trend as the liver, but values of TWI Targ-NPs and TWI Controls mice remained lower compared to the liver, not reaching the HET-UT and not being significantly different from the TWI-UT (Fig. 5E). Concerning sciatic nerve and spinal cord, instead, we did not observe any significantly detectable GALC activity neither in TWI Targ-NPs nor in TWI Controls (Fig. 5, F and G).

Last, we visualized the presence of NPs in the brain and liver by fluorescence confocal microscopy. As shown in Fig. 5H, we could detect the presence of fluorescently labeled NPs in the brain of mice treated with the three differently targeted GALC CLEA NPs. On the contrary, we could not find any NP fluorescence signal for mice treated with nonfunctionalized NPs. Livers were taken as positive controls and, as expected, presented a clear NP fluorescence both in the case of mice treated with targeted and nontargeted NPs.

Together, these data demonstrate that targeted GALC CLEAs NPs can induce GALC enzymatic activity via systemic administration in TWI brains up to the level required for the disease not to manifest. As expected, the presence of NPs was detected also in accumulation organs, while the spinal cord and sciatic nerves were not effectively treated.

DISCUSSION

In this study, we aimed to investigate the efficacy of CNS-targeted GALC-loaded biodegradable NPs as ERT agents for KD both in vitro and in vivo. The final objective of this work was to determine whether the targeted versions of our drug delivery system could reach the CNS of the mouse model for KD and promote enzymatic activity recovery in the brain, where GALC activity is most needed (*23*).

We tested three different peptides with potential as CNS-targeting agents, namely, Ang2, g7, and Tf2. Ang2 is a 19–amino acid peptide that promotes brain targeting as it binds the low-density lipoprotein receptor–related protein 1 (*14*). The efficacy of this peptide as a CNS-targeting agent has been extensively demonstrated with the Ang2-paclitaxel conjugate ANG1005, currently not only in preparation for the phase 3 clinical trial (*24*) but also in Ang2-modified nanostructures, including NPs (*25*). The g7 peptide is a glycosylated 7–amino acid–long peptide derived from the synthetic opioid peptide MMP-2200. Polymeric NPs bearing g7 peptide on the surface have been shown to cross the BBB with a mechanism that is still unclear, probably involving membrane-membrane interactions and micropinocytosis-related processes (*15*). Recently described peptide Tf2 allows indirect targeting of the transferrin receptor by recognizing transferrin and has the potential to target the CNS, given the high density of the transferrin receptor on the BBB (*16*).

We modified our previously developed NP formulation (*13*) based on CLEAs formation and encapsulation into PLGA NPs with each one of these three peptide ligands. The presence of targeting ligands on the NP surface led to an increase of the NP hydrodynamic diameter, particularly for NPs functionalized with the Ang2 peptide.

Although all the formulations could successfully encapsulate GALC, encapsulation efficiency varied among the NP compositions. Ang2- and Tf2-functionalized NPs showed a lower encapsulation efficiency compared to g7-targeted NPs (60, 39, and 74%, respectively). Further evaluations are required to rationalize this observation, but it is worth noting that both Ang2 and Tf2, which show lower encapsulation efficiency, are also positively charged at neutral pH and have a higher isoelectric point (9.33 and 9.08, respectively, versus 5.98 of g7). It is possible that unfavorable electrostatic interactions take place during the enzyme encapsulation process, leading to a poorer outcome. However, Ang2 and Tf2 NPs resulted in a higher activity yield of GALC CLEAs (61 and 67%, respectively) compared to GALC g7 NPs (37%). Even in this case, the different peptide environment could lead to different exposure of the enzyme to the outer medium or cause undesired interactions between the targeting peptide and the enzyme. All in all, despite small differences in terms of encapsulation efficiency and activity yield, the presence of targeting ligands did not represent an obstacle in the encapsulation of active GALC CLEAs in NPs of suitable size (*26*).

Before testing the potential of the NP formulations as ERT candidates, we verified that all NP types could enter cells and reach the intracellular target of GALC, which is represented by lysosomes, a key point to be investigated since endocytic route and signaling can be severely altered in most LSDs (*20*). Confocal images and colocalization analysis confirmed that all the NPs used in this study were taken up by cells and were localized into lysosomes 24 hours upon treatment. This was independent of the type of ligand and also of the type of cell, since similar results were obtained in TWI and WT fibroblasts. This means that, while the targeting peptides should address NPs to a certain district in the organism, at the cellular level, they do not affect the expected fate of NPs, which in this case leads to the endolysosomal route (*27*). Together, our results indicate that GALC CLEA NPs can successfully vehiculate the enzyme inside cells and accumulate in the lysosomes, where GALC is supposed to perform its physiological activity, and that the preferred localization of delivered GALC in the lysosomes is not affected by the presence of targeting ligands on the carrier's surface.

Thus, we proceeded with testing the ability of all NPs formulations to deliver enzymatically active GALC in cells. A dose-response experiment revealed that all formulations could promote enzymatic activity in primary murine GALC-deficient cells in a dose-dependent manner. The recombinant enzyme administered alone provided cells with an activity that was always lower than the one resulting from the corresponding NP dose. NP doses of 3 and 6 U allowed performing efficient ERT in vitro, bringing enzymatic cell activity equal or even higher than the physiological activity of healthy cells, while not even the highest dose of free rm-GALC could induce WT activity. These data prove the effectiveness of our NPs to deliver GALC inside cells in an active form and in a more efficient way if compared to the nonencapsulated enzyme. This behavior can be probably attributed to the known ability of polymeric NPs to protect the enzyme before it reaches the lysosomes (*28*) and to the capability of controlling the release of their cargo at the lysosomal acidic pH (*29*). Moreover, a time-response experiment showed that targeted NPs can maintain constant GALC activity (equal or higher than WT) between 24 and 96 hours after treatment. Nontargeted NPs, instead, were affected by an activity decrease at $t = 96$ hours. These results suggest that targeting agents could enhance NPs persistence inside cells (*30*). Free rm-GALC, rather, yielded less than 50% of WT activity after 24 hours and reached the WT level only after 96 hours. These in vitro data add important information to the very little knowledge present in the literature about the suitability of polymeric NPs for

ERT. To date, only a few works have investigated the capability of PLGA NPs to deliver functional enzymes, and only in vitro (*13*, *28*). In this context, our results confirm the potential of NPs made of this material for enzyme delivery in vitro.

Given the very promising in vitro data, we proceeded with the testing of our NP formulations in vivo in the TWI mouse, an authentic mouse model of KD. TWI mice are by far the most commonly used murine model in KD research, owing to the fact that this model closely recapitulates human conditions such as undetectable GALC activity, PSY accumulation in CNS and PNS, white matter degeneration, and the presence of globoid cells. We treated TWI mice intraperitoneally with a single NP injection to later assay the GALC activity inside different organs (of CNS or PNS and in accumulation organs). We preliminarily carefully evaluated different routes of drug administration, and we decided to use intraperitoneal injection given that is the predominantly used method for systemic drugs administration in small mice and that allows administering large volumes of fluid safely. As expected, we found substantial GALC activity in the examined accumulation organs (*10*, *31*). Both targeted (Ang2, g7, or Tf2) GALC CLEA NPs and controls (nontargeted NPs and rm-GALC) accumulated in a similar amount in the liver and kidneys 4 hours after injection. These generally high liver accumulations confirm the effectiveness of intraperitoneal injection. Intraperitoneally injected drugs, indeed, are primarily absorbed by mesenteric vessels, which drain into the portal vein, pass through the liver, and lastly reach the systemic circulation (*32*). Regarding the brain, instead, we found that mice treated with targeted NPs displayed a GALC activity that was approximately equal to the activity of the HET-UT mice (heterozygous mice for GALC mutation). This is a key finding if considered that heterozygous mice are characterized by a completely healthy phenotype. The same is valid for human carriers of GALC mutations. This result is even more appealing, considering that brains of mice treated with nontargeted NPs or with the free enzyme instead did not show any significant GALC activity increase. The fact that GALC activity was not found in the brains of mice treated with nontargeted NPs but was instead present in their livers confirms that, after reaching systemic circulation, BBB passage can be attributed to the mechanism of the specific targeting peptides, which have been already extensively investigated by us and others (*14*–*16*). Although some studies demonstrated the ability of different types of NPs to reach the brain, this is the first time that a nanovector is shown to deliver a functional enzyme into the brain of an LSD model. Several efforts have been made to exploit certain cell receptors to allow a free native or modified enzyme to pass the BBB, but with not very promising results (*33*, *34*). Even if the enzyme could reach the brain, in fact, it would be rapidly metabolized by cells, causing the need for very frequent injections from the perspective of clinical treatment. Despite the fact that ERT with free recombinant enzymes is the most widely applied clinical method to treat non-CNS–involved LSDs, it requires long-term and frequent treatments, resulting in expensive therapies that are not free from side effects, including immunoreactions (*35*). In this context, the possibility to perform ERT with the enzyme encapsulated in a safe nanovector is definitely appealing, as it could protect and slowly release the enzyme, thus minimizing some of the classical ERT disadvantages.

Concerning the other analyzed tissues of the nervous system (the spinal cord and sciatic nerve), neither enzyme-loaded NPs nor the recombinant enzyme could induce a significant GALC activity increase. This is actually not unexpected. It is known indeed that efficient drug delivery of therapeutic doses to these districts can be difficult to achieve, owing to neuroanatomy issues and the restrictiveness of the blood-nerve barrier (*36*). A time longer than 4 hours would be likely necessary to appreciate an elevation of the enzyme activity also in these areas. There is also the possibility that different targeting strategies may be required. Specific studies to address this point will be necessary, being that the involvement of PNS is another typical feature of KD and many other LSDs.

Two other important aspects that deserve to be underlined concern interbatch reproducibility and the effect of cell sex on uptake of NPs. Regarding the first one, all the in vivo experiments of this work were carried with two different NP batches, each one independently synthesized (i.e., in different days), with lots of different recombinant enzyme. Results were perfectly consistent among the two batches. This observation gives an adjunctive strength to our approach, demonstrating the reproducibility also among different batches of the produced drug. Interbatch reproducibility is indeed a very critical point regarding NPs in general. For this reason, for example, many efforts have been recently made to construct chips capable of automatically synthesizing polymeric NPs in a very reproducible way (*37*). Cell sex, instead, is an interesting overlooked factor, which can affect NP uptake by cells. Recently, in fact, Serpooshan and co-workers demonstrated that cell sex leads to differences in quantum dot uptake between male and female human amniotic stem cells and primary fibroblasts (*38*). These findings lay the foundation for the fact that variations existing in the production of paracrine factors (as proteins or hormones) by male and female cells may have the capacity to modify the protein corona of NPs, potentially affecting NP cell interactions. However, mice treated with our targeted NPs formulations did not report significant different outcomes between male and female animals. Targeting peptides, thus, seem to promote BBB translocation in a sex-independent manner, in accordance with the fact that also enzyme release from our targeted NPs is not markedly affected by the presence of the protein corona. Nevertheless, given the difference in cell-secreted molecules that can occur between organisms with different sexes during life, a longitudinal study of this aspect would be desirable in view of an effective treatment.

Last, to underline the potential of clinical translatability of this drug delivery system, we also performed a test in human cells derived from patients with KD carrying the 30-kb deletion in the GALC gene, one of the most common mutations causing KD (*39*). NPs revealed to be able to carry enzymatically active GALC very efficiently also into human cells, providing them with a GALC enzymatic activity that was much higher than that of healthy cells up to 96 hours after the treatment. For comparison, free rm-GALC could not even provide 50% of the activity of healthy cells. This confirms the potential of GALC CLEA NPs for ERT also in a human KD physiological environment.

In view of a clinical translation, a possible technical limitation that is also common to other ERT approaches for other rare diseases might be the availability of a large amount of drug allowing for treatment of the patient for a lifetime. Producing recombinant enzymes from eukaryotic cells, in fact, remains a quite expensive process (*40*). If this was the case, NP-mediated ERT could be decisive if used as a sort of "buffer therapy" to be promptly applied to the child immediately after birth for a limited period of time, in combination with other therapeutic approaches. In this way, a physiological enzyme activity would avoid nervous system damage before the "long-term therapy" (most likely GT) can engraft and provide its therapeutic effect (*41*). Last, we should stress that developing a therapy preventing all neural damages is a markedly challenging task in KD. It is indeed very rapidly progressing, with a median age of symptom onset of 4 months and median time to diagnosis after onset of 3 months. Therefore, to have a chance of success, it is imperative that therapy must

guarantee GALC activity in the CNS and PNS as soon as possible. Consequently, also a deeper understanding of disease progression in early-onset KD is critical for developing treatments, designing clinical trials, and evaluating outcomes.

In conclusion, with this study, we demonstrated the capability of targeted polymeric NPs to perform delivery of a protein into the brain of a murine model of LSD, overcoming the BBB and delivering functional enzyme in a therapeutically relevant amount. This effective approach opens new exciting therapeutic opportunities not only for all CNS-involved LSDs with no cure available to date but also for all disorders, which could benefit from the passage of specific proteins through the BBB to reach CNS.

MATERIALS AND METHODS

Materials

PLGA (Resomer RG 503H and Resomer RG 752H) was purchased from Sigma-Aldrich and used as received. ATTO 488–NHS ester and Atto 633 amine were purchased from ATTO-TEC GmbH (Germany) and used as stock solutions (10 mg/ml) in dimethyl sulfoxide (DMSO).

All other chemicals were purchased from Sigma-Aldrich, unless otherwise specified. All chemicals were used as received.

Methods

PLGA-NHS synthesis

PLGA was activated via NHS 1-ethyl-3-(3-dimethylaminopropyl) carbodiimide (EDC) chemistry. PLGA (0.05 mmol) were dissolved in 5 ml of anhydrous dichloromethane (DCM) under nitrogen atmosphere, and 0.5 mmol of NHS was added. Then, 0.5 mmol of EDC-HCl and 0.6 mmol of triethylamine (TEA) were added. The reaction mix was stirred for 18 hours at room temperature, and the product was precipitated with methanol and collected by centrifugation. The final product was washed twice with methanol, then characterized by ^{1}H NMR (nuclear magnetic resonance) in $CDCl_3$, and stored at −20°C until use. Characterization: ^{1}H NMR (300 MHz, $CDCl_3$; Bruker Avance 300 spectrometer): δPLGA-NHS = 5.2 parts per million (ppm) [—$OCH(CH_3)COO$—], 4.8 ppm [—OCH_2COO—], 2.9 ppm [—$COCH_2CH_2COON$—), and 1.6 ppm [—$OCH(CH_3)CO$—].

PLGA-Mal synthesis

PLGA-NHS was further modified with a maleimide group to allow the reaction with cysteine-terminated peptides. PLGA-NHS (0.05 mmol) was dissolved in DCM, and 0.1 mmol of *N*-(2-aminoethyl)maleimide trifluoroacetate was added together with 0.11 mmol of TEA. The reaction mix was stirred for 2 hours at room temperature, and the product was precipitated with methanol and collected by centrifugation. The final product was washed twice with methanol and characterized by ^{1}H NMR (300 MHz, $CDCl_3$; Bruker Avance 300 spectrometer): δPLGA-Mal = 6.7 ppm (—HC—CH—), 5.2 ppm [—$OCH(CH_3)COO$—], and 1.6 ppm [—$OCH(CH_3)CO$—].

Peptide-modified PLGA synthesis

All peptides used in this study were synthesized via solid phase peptide synthesis as described elsewhere (*15*, *16*).

The peptide sequences are the following:

1) Ang2: TFFYGGSRGKRNNFKTEEYGC
2) g7: GF(D-)TGFLS(O-β-D-glucose)
3) Tf2: CGGGHKYLRW

Peptide (2.25 μmol) was added to 2.05 μmol of PLGA-NHS (for g7-PLGA synthesis) or PLGA-Mal (for Ang2-PLGA and Tf2-PLGA synthesis) in *N*,*N*′-dimethylformamide. The mixture was stirred at room temperature for 18 hours (g7-PLGA) or 48 hours (Ang2-PLGA and Tf2-PLGA). The final product was precipitated with methanol, collected by centrifugation, and washed twice with methanol. The reactions were monitored via ^{1}H NMR in $CDCl_3$ (300 MHz; Bruker Avance 300 spectrometer) until the absence of the NHS or the maleimide group δ, indicating complete conversion. The final products were dried and stored at −20°C until use.

Fluorophore-tagged PLGA synthesis

ATTO 633 amine (0.24 μmol) was added to 0.22 μmol of PLGA-NHS in DMSO. The mixture was stirred for 18 hours at room temperature, and the final product was precipitated with methanol and collected by centrifugation. The obtained labeled PLGA was washed twice with methanol, dried, and stored at −20°C until use.

rm-GALC production

Human embryonic kidney 293T cells stably expressing and secreting His6-tagged murine WT GALC (provided by J. Deane of the Cambridge University) (*42*) were maintained in 400 μM zeocin selection medium and expanded in 1450-cm^2 inner surface roller bottles (37°C, 5% CO_2, 0.7 rpm). The enzyme was routinely purified from extracellular medium by nickel affinity chromatography (Ni Sepharose excel histidine-tagged protein purification resin; 17-3712-03, GE Healthcare Life Sciences) as in (*13*). The purified enzyme was lastly buffer-exchanged with 10 kDa molecular mass cut-off concentrator and stored at −20°C until use.

CLEAs synthesis

To produce GALC CLEAs, typically 200 μl of GALC solution [750 μg/ml in 10 mM mannitol, 5 mM glycine, 140 mM NaCl, 3.7 mM sodium phosphate buffer, and 0.05% Tween 80 (pH 5.5)] was added to 600 μl of acetone simultaneously with 2 μl of 25% glutaraldehyde under stirring. The mixture was then stirred overnight at 4°C. The formed CLEAs were centrifuged (30 min, 4°C, 13200 rpm) and washed twice with 1 ml of acetone. The final GALC CLEAs were suspended in 1 ml of acetone and stored at −20°C until use. To produce fluorescently labeled GALC CLEAs, ATTO 488–NHS solution in DMSO (10 mg/ml) was added to 1 ml of GALC CLEAs with 1:20 CLEAs:ATTO 488–NHS molar ratio. The mixture was stirred for 4 hours at room temperature, centrifuged (30 min, 13200 rpm), and washed twice with 1 ml of acetone. Resulting ATTO 488–tagged CLEAs were suspended in 1 ml of acetone and stored at −20°C until use.

CLEA NPs synthesis

For targeted NP synthesis, 200 μl of GALC CLEAs were added to 200 μl of a solution containing 8 mg of PLGA 752H and 2 mg of peptide-modified PLGA in acetone. This mixture was then added dropwise to 1200 μl of 2% sodium cholate in water under stirring. The formed NP suspension was centrifuged (20 min, 4°C, 13200 rpm) and washed twice with 500 μl of water. The final NP pellet was suspended in 50 μl of D-(+)-trehalose (100 mg/ml) and stored at −20°C until use. To produce nontargeted NPs, peptide-modified PLGA was replaced with the same amount of PLGA 503H.

Fluorescently labeled NPs were obtained, adding 0.1 mg of ATTO 633–tagged PLGA and replacing GALC CLEAs with ATTO 488–tagged GALC CLEAs. Empty NPs were produced, replacing GALC CLEAs with the same volume of acetone.

Hydrodynamic diameter and zeta potential

Hydrodynamic diameter and zeta potential of NPs were measured with a Zetasizer NanoZS (Malvern Instruments Inc., UK) by means of dynamic light scattering. Samples were diluted 1:1000 in deionized water before measurement. Samples were transferred into polypropylene cuvettes for hydrodynamic diameter measurement or into appropriate electrophoretic cells for zeta potential determination. Measurements were performed at room temperature. Mean hydrodynamic diameter resulted from the autocorrelation function of the intensity

of scattered light calculated by DTS Nano software. Electrophoretic mobility was determined and converted into zeta potential by DTS Nano software.

Protein quantitation

GALC concentration in NP samples was determined via ninhydrin assay. Briefly, 5 µl of NPs were digested overnight at 95°C in 200 µl of 6 M HCl and then vacuum dried. The residue was suspended in deionized water, and 10 µl of each sample was added to 110 µl of ninhydrin reagent [ninhydrin (20 mg/ml) and stannous chloride (2 mg/ml) in 75% ethylene glycol in 4N acetate buffer (pH 5.5)]. The reaction mixture was heated at 95°C for 20 min, and samples were plated into a 96-well microplate. Absorbance was measured at 560 nm.

Protein concentration was calculated by interpolation from a calibration curve prepared with GALC subject to the same digestion and reaction protocols.

NP encapsulation efficiency was determined as follows

$$EE\% = \frac{GALC(\mu g)_{NPs}}{GALC(\mu g)_{INJ}} \cdot 100$$

where $GALC(\mu g)_{NPs}$ is the amount of GALC encapsulated in NPs and $GALC\ (\mu g)_{INJ}$ is the amount of GALC used in each synthesis.

GALC activity measurement in NPs

To determine GALC activity in NP samples, 2 µl of NPs was added to 50 µl of assay buffer [50 mM sodium citrate, 125 mM NaCl, and 0.5% Triton X-100 (pH 4.5)]. Then, 50 µl of 1 mM 4-methylumbelliferyl-β-D-galactopyranoside in assay buffer was added. Samples were incubated at 37°C for 20 min, and 200 µl of stop solution (0.5 M glycine, 0.3 M NaOH) was added. Samples were plated into a 96-well multiplate for fluorescence, and fluorescence was measured with the Promega GloMax discover Multimode microplate reader with an excitation filter of 365 nm and an emission filter of 415 to 485 nm.

Activity yield (AY%) of NPs was calculated as the ratio between the specific activity of the sample (SA_{NPs}) and the specific activity of the unaltered GALC (SA_{GALC}) as follows

$$AY\% = \frac{SA_{NPs}}{SA_{GALC}} \cdot 100$$

where the specific activities are defined as unit of enzyme (U) per microgram of enzyme (μg_{GALC})

$$SA = \frac{U}{\mu g_{GALC}}$$

One unit of enzyme (U) is defined as 1 nmol of substrate ($nmol_{SUB}$) hydrolyzed in 1 hour

$$1U = \frac{1\ nmol_{SUB}}{h}$$

Primary human and murine cell cultures and treatments

Adult mouse fibroblast cultures were obtained from WT and TWI ears, according to the protocol established in the laboratory of E. Eichler (University of Washington; https://genome.ucsc.edu/ENCODE/protocols/cell/mouse/Fibroblast_Stam_protocol.pdf) with minor modifications. Briefly, after anesthesia, mouse ears were extracted, washed with sterile water, and cut into small pieces. All pieces were then collected in a tube and added with collagenase XI (C7657-100 mg; Sigma-Aldrich) diluted in high glucose Dulbecco's modified Eagle medium (DMEM) [approximately 2.5 mg of collagenase, 320 collagen digestion units (CDU), for one mouse]. After 2 hours of incubation at 37°C, the Eppendorf tube was centrifuged for 5 min at 200*g*, the supernatant was discarded, and the pellet was washed with 2 ml of PBS and centrifuged again, discarding the supernatant. Trypsin-EDTA 0.05% (59418C-100ML, Thermo Fisher Scientific) was then added to the tube and left for 45 min at 37°C. The tube was then centrifuged, and the pellet was resuspended in the complete DMEM [high-glucose DMEM supplemented with 10% of heat-inactivated fetal calf serum (FCS), 4 mM L-glutamine, and 1% penicillin/streptomycin; all products were from Gibco, Life Technologies)]. Obtained cells were thus dissociated, pipetting up and down with a 10-ml syringe (with a 21 gauge needle), plated in a 60-mm cell petri dish, and incubated at 37°C in a humidified atmosphere containing 5% CO_2. The day after, cells were washed, and medium was replaced. After reaching confluence (approximately 3 to 4 days), cells (p0) were washed with 1 ml of PBS and split with a ratio of 1:2. Human fibroblasts [from an HD (C0045C, Life Technologies) and from a patient with the large common Caucasian 30-kDa deletion in the GALC gene, c.1161+6532_polyA+9kbdel (30kbΔ; F0461990, Gaslini Institute Biobank)] (*39*) were donated by Gritti (San Raffaele Telethon Institute for Gene Therapy, Milan, Italy) and maintained under the just mentioned culture conditions. For experiments, WT, TWI, 30kbΔ, and HD fibroblast cells were plated in standard 96-well cell plates (12,500 cell per well). Twenty-four hours later, medium was replaced with fresh medium containing NPs at different concentrations. After 4 hours of NPs incubation, medium was removed, and cells were washed three times with 100 µl of PBS. Then, cells were lysed for the enzymatic assay or fresh medium was added, and cells were lysed after 24 or 96 hours. For every NP experiment, male and female strains were used for experiments with mice cells; a female strain was used for experiments with human cells. WT and TWI cells were used at passage 4, and 30kbΔ and HD cells were used at passage 8 (*43*).

GALC enzymatic activity assay in cell and tissues

GALC enzymatic activity assay was carried out both in murine/human fibroblasts and mouse tissues (brain, liver, kidney, sciatic nerve, and spinal cord). Both primary cells and tissues were lysed on ice with radioimmunoprecipitation assay (RIPA) buffer (Sigma-Aldrich) containing a protease and phosphatase inhibitors cocktail (cOmplete and PhosSTOP, Roche Diagnostics). Cell lysates were sonicated (for 4 s at 12 µm of intensity), whereas tissues were homogenized in 1.5 ml of Eppendorf tube with appropriate micropestles. Then, after centrifugation (15,000*g* for 25 min at 4°C), the supernatants were collected and tested for protein concentration by the micro-bicinchoninic acid (BCA) Protein Assay Kit (Thermo Scientific Pierce). To measure GALC activity, we used 6-hexadecanoylamino-4-methylumbelliferyl-β-D-galactopyranoside (HMU-βGal), the fluorescent substrate currently used for the clinical diagnosis of KD (*44*): 10 µl of lysates was added to 20 µl of 50 µM HMU-βGal substrate solution, incubated for 17 hours at 37°C. The reaction was then stopped, and the fluorescent product [4-methylumbelliferone (4-MU)] was read by using the microplate GloMax fluorescence reader. GALC activity (reported as nanomole per milligram protein extract in 17 hours of incubation) was calculated by comparison with a standard curve previously obtained by measuring the fluorescence of different concentration of 4-MU.

Animal procedures

TWI heterozygous mice ($TWI^{+/-}$ C57BL6 mice; the Jackson Laboratory), donated by A. Biffi (San Raffaele Telethon Institute for

Gene Therapy, Milan, Italy), were used as breeder pairs to generate homozygous TWI mice ($TWI^{-/-}$, elsewhere abbreviated as TWI for simplicity). Animals were maintained under standard housing conditions and used according to the protocols and ethical guidelines approved by the Ministry of Health (permit no. Codice 535/2018-PR; official starting date: 9 July 2018). For genotyping purpose, mice genomic DNA was extracted from clipped tails of mice at post-natal day (PND) 10 to 15 (EUROGOLD Tissue-DNA Mini Kit, EUROCLONE), as previously done by us (*45*). The genetic status of each mouse was later determined from the genome analysis of the TWI mutation, as reported from Sakai and co-workers (*46*). TWI, WT, and HET animals (PND 19 to 21) were used for experiments. TWI animals were intraperitoneally injected with NPs (1600 mg/kg) or with free GALC (100 mg/kg) diluted in 1 ml of physiological solution (*3*, *47*). After 4 hours, mice were deeply anesthetized with a urethane solution (0.8 ml/Hg; Sigma-Aldrich) and euthanized by transcardial perfusion with PBS so as to remove the blood from vessels. Subsequently, the brain and liver were extracted from each mouse, and one brain hemisphere or liver lobe was placed in 4% PFA solution and the other hemisphere or liver lobe in RIPA lysis buffer (R0278-50ML, Sigma-Aldrich) containing a protease and phosphatase inhibitors cocktail [cOmplete (4693116001) and PhosSTOP (4906845001), Roche Diagnostics]. The spinal cord, sciatic nerve, and kidneys were also extracted and stored in the complete RIPA buffer previously described. Last, organs placed in the PFA solution were stored at 4°C for a minimum of 3 days before vibratome cutting, whereas organs put in the lysis buffer were immediately processed to perform the GALC enzymatic assay. Regarding mice sex, experiments were done as follows: First, five WT male, seven WT female, four TWI male, three TWI female, one HET male, and two HET female were used for the untreated conditions. Second, three TWI male and three TWI female were used for the targeted-GALC loaded NPs injections (one male and one female for each targeting peptide: g7, ANG2, or Tf2). Last, two TWI male and two TWI female were used for the control conditions (one male and one female for nontargeted GALC-loaded NPs and for the free GALC). All procedures were made with the maximal efforts to minimize mice suffering.

Cells and tissues confocal imaging

TWI or WT fibroblasts were seeded 24 hours before experiments into a glass-bottom petri dish (WillCo-dish GWST-3522) to reach 80 to 90% confluence. Incubation with targeted or nontargeted GALC-loaded NPs was performed at 37°C with 5% CO_2 in DMEM with 10% FCS at final NP concentration of 1.5 mg/ml. After 4 hours, cells were washed twice with PBS and incubated with fresh medium for 20 hours. Then, cells were incubated with 0.1 μM LysoTracker Red DND-99 (Thermo Fisher Scientific). After 15 min, cells were washed with PBS and stained with 4% PFA before imaging.

For tissue imaging, the brain and liver samples were processed as described in the animal procedure paragraph. Samples were cut with a vibratome (Leica VT1000 S) at a final slice thickness of 60 μm. In particular, consecutive coronal brain sections were cut at 0.5 to 2.10 mm from bregma.

All samples were mounted with Fluoroshield mounting medium with 4′,6-diamidino-2-phenylindole. Samples were imaged with a Leica TCS SP5 SMD inverted confocal microscope (Leica Microsystems AG) interfaced with Ar, diode-pumped solid-state (DPSS), and HeNe lasers for excitation at 488, 560, and 633 nm, respectively, and with an external pulse diode laser for excitation at 405 nm. Samples were viewed with a 40× 1.5 numerical aperture oil immersion objective (Leica Microsystems) with pinhole aperture set at 1.0 Airy. All images were analyzed with Fiji software, and colocalization was determined with JACoP plugin.

Statistical analysis

If not differently specified, data are reported as means ± SEM obtained from at least three independent experiments (in figure legends, "*n*" indicates the number of experiments performed). Data were statistically analyzed by using Prism 6.00 (GraphPad Software, San Diego, CA; RRID:SCR_002798). For parametric data, Student's *t* test (unpaired, two tailed) or one-way analysis of variance (ANOVA) (Tukey's or Dunnett's multiple comparisons test) was used; the mean values obtained in each repeated experiment were assumed to be normally distributed about the true mean. Statistical significance refers to results for which $P < 0.05$ was obtained.

SUPPLEMENTARY MATERIALS

Supplementary material for this article is available at http://advances.sciencemag.org/cgi/content/full/5/11/eaax7462/DC1

Fig. S1. Intracellular localization of targeted GALC CLEA NPs in WT cells.

Fig. S2. Untreated WT and TWI fibroblasts.

Fig. S3. GALC-loaded NPs activity over time in the presence and absence of serum proteins.

View/request a protocol for this paper from *Bio-protocol*.

REFERENCES AND NOTES

1. S. U. Walkley, Pathogenic cascades in lysosomal disease—Why so complex? *J. Inherit. Metab. Dis.* **32**, 181–189 (2009).
2. A. Del Grosso, S. Antonini, L. Angella, I. Tonazzini, G. Signore, M. Cecchini, Lithium improves cell viability in psychosine-treated MO3.13 human oligodendrocyte cell line via autophagy activation. *J. Neurosci. Res.* **94**, 1246–1260 (2016).
3. F. Matthes, C. Andersson, A. Stein, C. Eistrup, J. Fogh, V. Gieselmann, D. A. Wenger, U. Matzner, Enzyme replacement therapy of a novel humanized mouse model of globoid cell leukodystrophy. *Exp. Neurol.* **271**, 36–45 (2015).
4. D. A. Wenger, M. A. Rafi, P. Luzi, J. Datto, E. Costantino-Ceccarini, Krabbe disease: Genetic aspects and progress toward therapy. *Mol. Genet. Metab.* **70**, 1–9 (2000).
5. M. L. Escolar, M. D. Poe, J. M. Provenzale, K. C. Richards, J. Allison, S. Wood, D. A. Wenger, D. Pietryga, D. Wall, M. Champagne, R. Morse, W. Krivit, J. Kurtzberg, Transplantation of umbilical-cord blood in babies with infantile Krabbe's disease. *N. Engl. J. Med.* **352**, 2069–2081 (2005).
6. A. Ricca, N. Rufo, S. Ungari, F. Morena, S. Martino, W. Kulik, V. Alberizzi, A. Bolino, F. Bianchi, U. Del Carro, A. Biffi, A. Gritti, Combined gene/cell therapies provide long-term and pervasive rescue of multiple pathological symptoms in a murine model of globoid cell leukodystrophy. *Hum. Mol. Genet.* **24**, 3372–3389 (2015).
7. A. M. Bradbury, M. A. Rafi, J. H. Bagel, B. K. Brisson, M. S. Marshall, J. Pesayco Salvador, X. Jiang, G. P. Swain, M. L. Prociuk, P. A. ODonnell, C. Fitzgerald, D. S. Ory, E. R. Bongarzone, G. D. Shelton, D. A. Wenger, C. H. Vite, AAVrh10 gene therapy ameliorates central and peripheral nervous system disease in canine globoid cell leukodystrophy (Krabbe Disease). *Hum. Gene Ther.* **29**, 785–801 (2018).
8. A. Safary, M. Akbarzadeh Khiavi, R. Mousavi, J. Barar, M. A. Rafi, Enzyme replacement therapies: What is the best option? *BioImpacts* **8**, 153–157 (2018).
9. R. Thomas, A. R. Kermode, Enzyme enhancement therapeutics for lysosomal storage diseases: Current status and perspective. *Mol. Genet. Metab.* **126**, 83–97 (2019).
10. S. Muro, New biotechnological and nanomedicine strategies for treatment of lysosomal storage disorders. *Wiley Interdiscip. Rev. Nanomed. Nanobiotechnol.* **2**, 189–204 (2010).
11. G. Sharma, A. R. Sharma, S.-S. Lee, M. Bhattacharya, J.-S. Nam, C. Chakraborty, Advances in nanocarriers enabled brain targeted drug delivery across blood brain barrier. *Int. J. Pharm.* **559**, 360–372 (2019).
12. T. Patel, J. Zhou, J. M. Piepmeier, W. M. Saltzman, Polymeric nanoparticles for drug delivery to the central nervous system. *Adv. Drug Deliv. Rev.* **64**, 701–705 (2012).
13. M. Galliani, M. Santi, A. Del Grosso, A. Cecchettini, F. M. Santorelli, S. L. Hofmann, J.-Y. Lu, L. Angella, M. Cecchini, G. Signore, Cross-Linked enzyme aggregates as versatile tool for enzyme delivery: Application to polymeric nanoparticles. *Bioconjug. Chem.* **29**, 2225–2231 (2018).
14. M. Demeule, J.-C. Currie, Y. Bertrand, C. Ché, T. Nguyen, A. Régina, R. Gabathuler, J.-P. Castaigne, R. Béliveau, Involvement of the low-density lipoprotein receptor-related protein in the transcytosis of the brain delivery vector Angiopep-2. *J. Neurochem.* **106**, 1534–1544 (2008).

15. G. Tosi, R. A. Fano, L. Bondioli, L. Badiali, R. Benassi, F. Rivasi, B. Ruozi, F. Forni, M. A. Vandelli, Investigation on mechanisms of glycopeptide nanoparticles for drug delivery across the blood–brain barrier. *Nanomedicine* **6**, 423–436 (2011).
16. M. Santi, G. Maccari, P. Mereghetti, V. Voliani, S. Rocchiccioli, N. Ucciferri, S. Luin, G. Signore, Rational design of a transferrin-binding peptide sequence tailored to targeted nanoparticle internalization. *Bioconjug. Chem.* **28**, 471–480 (2017).
17. T. Kobayashi, T. Yamanaka, J. M. Jacobs, F. Teixeira, K. Suzuki, The twitcher mouse: An enzymatically authentic model of human globoid cell leukodystrophy (Krabbe disease). *Brain Res.* **202**, 479–483 (1980).
18. N. Kamaly, G. Fredman, M. Subramanian, S. Gadde, A. Pesic, L. Cheung, Z. A. Fayad, R. Langer, I. Tabas, O. C. Farokhzad, Development and in vivo efficacy of targeted polymeric inflammation-resolving nanoparticles. *Proc. Natl. Acad. Sci.* **110**, 6506–6511 (2013).
19. S. Nagano, T. Yamada, N. Shinnoh, H. Furuya, T. Taniwaki, J.-i. Kira, Expression and processing of recombinant human galactosylceramidase. *Clin. Chim. Acta* **276**, 53–61 (1998).
20. F. Begarani, F. D'Autilia, G. Signore, A. Del Grosso, M. Cecchini, E. Gratton, F. Beltram, F. Cardarelli, Capturing metabolism-dependent solvent dynamics in the lumen of a trafficking lysosome. *ACS Nano* **13**, 1670–1682 (2019).
21. X. L. Meng, Y. Eto, R. Schiffmann, J. S. Shen, HIV tat domain improves cross-correction of human galactocerebrosidase in a gene- and flanking sequence-dependent manner. *Mol. Ther. Nucleic Acids* **2**, e130 (2013).
22. V. Mirshafiee, M. Mahmoudi, K. Lou, J. Cheng, M. L. Kraft, Protein corona significantly reduces active targeting yield. *Chem. Commun.* **49**, 2557–2559 (2013).
23. D. A. Wenger, *GeneReviews®* (University of Washington, 2011).
24. A. Régina, M. Demeule, C. Ché, I. Lavallée, J. Poirier, R. Gabathuler, R. Béliveau, J.-P. Castaigne, Antitumour activity of ANG1005, a conjugate between paclitaxel and the new brain delivery vector Angiopep-2. *Br. J. Pharmacol.* **155**, 185–197 (2008).
25. H. Xin, X. Jiang, J. Gu, X. Sha, L. Chen, K. Law, Y. Chen, X. Wang, Y. Jiang, X. Fang, Angiopep-conjugated poly(ethylene glycol)-co-poly(ε-caprolactone) nanoparticles as dual-targeting drug delivery system for brain glioma. *Biomaterials* **32**, 4293–4305 (2011).
26. J. W. Hickey, J. L. Santos, J.-M. Williford, H.-Q. Mao, Control of polymeric nanoparticle size to improve therapeutic delivery. *J. Control. Release* **219**, 536–547 (2015).
27. M. Galliani, C. Tremolanti, G. Signore, Nanocarriers for protein delivery to the cytosol: Assessing the endosomal escape of poly(Lactide-co-Glycolide)-poly(Ethylene Imine) nanoparticles. *Nanomaterials* **9**, E652 (2019).
28. J. M. Kelly, A. L. Gross, D. R. Martin, M. E. Byrne, Polyethylene glycol-b-poly(lactic acid) polymersomes as vehicles for enzyme replacement therapy. *Nanomedicine* **12**, 2591–2606 (2017).
29. A. Mühlstein, S. Gelperina, J. Kreuter, Development of nanoparticle-bound arylsulfatase B for enzyme replacement therapy of mucopolysaccharidosis VI. *Pharm.* **68**, 549–554 (2013).
30. D. Raucher, S. Dragojevic, J. Ryu, Macromolecular drug carriers for targeted glioblastoma therapy: Preclinical studies, challenges, and future perspectives. *Front. Oncol.* **8**, 624 (2018).
31. F. Umezawa, Y. Eto, T. Tokoro, F. Ito, K. Maekawa, Enzyme replacement with liposomes containing beta-galactosidase from Charonia lumpas in murine globoid cell leukodystrophy (twitcher). *Biochem. Biophys. Res. Commun.* **127**, 663–667 (1985).
32. P. V. Turner, T. Brabb, C. Pekow, M. A. Vasbinder, Administration of substances to laboratory animals: Routes of administration and factors to consider. *J. Am. Assoc. Lab. Anim. Sci.* **50**, 600–613 (2011).
33. A. Urayama, J. H. Grubb, W. S. Sly, W. A. Banks, Mannose 6-phosphate receptor-mediated transport of sulfamidase across the blood–brain barrier in the newborn mouse. *Mol. Ther.* **16**, 1261–1266 (2008).
34. R. J. Boado, Y. Zhang, Y. Zhang, C.-f. Xia, Y. Wang, W. M. Pardridge, Genetic engineering of a lysosomal enzyme fusion protein for targeted delivery across the human blood-brain barrier. *Biotechnol. Bioeng.* **99**, 475–484 (2008).
35. J. M. Kelly, A. Bradbury, D. R. Martin, M. E. Byrne, Emerging therapies for neuropathic lysosomal storage disorders. *Prog. Neurobiol.* **152**, 166–180 (2017).
36. K. A. Langert, E. M. Brey, Strategies for targeted delivery to the peripheral nerve. *Front. Neurosci.* **12**, 887 (2018).
37. M. Maeki, Microfluidics for pharmaceutical applications, in *Micro And Nano Technologies*, H. A. Santos, D. Liu, H. Zhang, Eds. (William Andrew Publishing, 2019), pp. 101–119.
38. V. Serpooshan, S. Sheibani, P. Pushparaj, M. Wojcik, A. Y. Jang, M. R. Santoso, J. H. Jang, H. Huang, R. Safavi-Sohi, N. Haghjoo, H. Nejadnik, H. Aghaverdi, H. Vali, J. M. Kinsella, J. Presley, K. Xu, P. C.-M. Yang, M. Mahmoudi, Effect of cell sex on uptake of nanoparticles: The overlooked factor at the nanobio interface. *ACS Nano* **12**, 2253–2266 (2018).
39. B. Tappino, R. Biancheri, M. Mort, S. Regis, F. Corsolini, A. Rossi, M. Stroppiano, S. Lualdi, A. Fiumara, B. Bembi, M. Di Rocco, D. N. Cooper, M. Filocamo, Identification and characterization of 15 novel GALC gene mutations causing Krabbe disease. *Hum. Mutat.* **31**, E1894–E1914 (2010).
40. R. H. Lachmann, Enzyme replacement therapy for lysosomal storage diseases. *Curr. Opin. Pediatr.* **23**, 588–593 (2011).
41. N. Yamazaki, M. Kosuga, K. Kida, G. Takei, Y. Fukuhara, H. Matsumoto, M. Senda, A. Honda, A. Ishiguro, T. Koike, H. Yabe, T. Okuyama, Early enzyme replacement therapy enables a successful hematopoietic stem cell transplantation in mucopolysaccharidosis type IH: Divergent clinical outcomes in two Japanese siblings. *Brain Dev.* **41**, 546–550 (2019).
42. J. E. Deane, S. C. Graham, N. N. Kim, P. E. Stein, R. McNair, M. B. Cachón-González, T. M. Cox, R. J. Read, Insights into Krabbe disease from structures of galactocerebrosidase. *Proc. Natl. Acad. Sci. U.S.A.* **108**, 15169–15173 (2011).
43. M. Mahmoudi, Debugging nano–bio interfaces: Systematic strategies to accelerate clinical translation of nanotechnologies. *Trends Biotechnol.* **36**, 755–769 (2018).
44. G. Wiederschain, R. Srinivasa, E. Kolodny, Characterization of 6-hexadecanoylamino-4-methylumbelliferyl-β-D-galactopyranoside as fluorogenic substrate of galactocerebrosidase for the diagnosis of Krabbe disease. *Clin. Chim. Acta* **205**, 87–96 (1992).
45. A. Del Grosso, L. Angella, I. Tonazzini, A. Moscardini, N. Giordano, M. Caleo, S. Rocchiccioli, M. Cecchini, Dysregulated autophagy as a new aspect of the molecular pathogenesis of Krabbe disease. *Neurobiol. Dis.* **129**, 195–207 (2019).
46. N. Sakai, K. Inui, N. Tatsumi, H. Fukushima, T. Nishigaki, M. Taniike, J. Nishimoto, H. Tsukamoto, I. Yanagihara, K. Ozono, S. Okada, Molecular cloning and expression of cDNA for murine galactocerebrosidase and mutation analysis of the twitcher mouse, a model of Krabbe's disease. *J. Neurochem.* **66**, 1118–1124 (1996).
47. P. Zhou, T. An, C. Zhao, Y. Li, R. Li, R. Yang, Y. Wang, X. Gao, Lactosylated PLGA nanoparticles containing ε-polylysine for the sustained release and liver-targeted delivery of the negatively charged proteins. *Int. J. Pharm.* **478**, 633–643 (2015).

Acknowledgments: We thank J. Deane for giving the 293T cells stably expressing rm-GALC and A. Gritti for giving the KD and HD patient's fibroblasts. **Funding:** This research was supported by European Leukodystrophy Association (ELA) International, under the framework of the project "Development of a novel, nanovector-mediated enzyme replacement therapy for Globoid Cell Leukodystrophy (GLD)", grant no. ELA 2015-010C1A. **Author contributions:** All authors had full access to all the data in the study and take responsibility for the integrity of the data and the accuracy of the data analysis. Study concept and design: A.D.G., M.G., M.C., and G.S. Acquisition of data: A.D.G., M.G., L.A., G.P., and M.S. Analysis and interpretation of data: All authors. Drafting of the manuscript: All authors. Statistical analysis: A.D.G., M.G., M.C., and G.S. Obtained funding: M.C. Study supervision: M.C. and G.S. **Competing interests:** The authors declare that they have no competing interests. **Data and materials availability:** All data needed to evaluate the conclusions in the paper are present in the paper and/or in the Supplementary Materials. Additional data related to this paper may be requested from the authors.

Submitted 18 April 2019
Accepted 19 September 2019
Published 20 November 2019
10.1126/sciadv.aax7462

Citation: A. Del Grosso, M. Galliani, L. Angella, M. Santi, I. Tonazzini, G. Parlanti, G. Signore, M. Cecchini, Brain-targeted enzyme-loaded nanoparticles: A breach through the blood-brain barrier for enzyme replacement therapy in Krabbe disease. *Sci. Adv.* **5**, eaax7462 (2019).